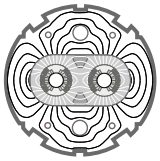

LHC Project Note 263

02 July 2001
Bernard.Jeanneret@cern.ch

Cascade simulation studies for the momentum cleaning insertion of LHC

I.L. Azhgirey*, I.S. Baishev*, J.B. Jeanneret, I.A. Kourotchkine* and G.R. Stevenson

Keywords: optics, collimation, cascade, radiation, dose, IR3

Summary

This note describes the details and the first results of the cascade simulations in the momentum cleaning section. The simulation scheme is the same as in the previous studies for the betatron cleaning insertion. Annual doses to the magnet coils are estimated from the calculated energy deposition densities assuming primary losses of 10^{16} 7 TeV protons per beam and per year in the momentum collimators. Shielding screens and insertions to reduce high doses to the coils of separation and corrector dipoles are discussed. The parameters of lateral leakage of hadrons are presented and compared to the same data for the betatron cleaning insertion.

1 Introduction

The design of the momentum cleaning system in IR3 is similar to the design of the related betatron cleaning system in IR7. The same principles of two-stage collimation are used[1, 2]. The basic layout of IR3 and IR7 is similar but the optics functions are different. For these reasons only the methods and some basic results of the radiation studies for IR7 [3, 4, 5, 6] are applicable to IR3 rather than the detailed results. In this study, the first working version V6.2 of the optics is used.

Our scheme of the cascade simulation in the entire momentum cleaning section follows the scheme detailed in [4]. First the cleaning process is simulated to define the map of primary inelastic interactions in the collimator jaws. Then a series of cascade calculations uses the above map as a source term together with a detailed geometrical model of the cleaning section. The energy deposition density in the magnet coils and hadron fluence

*Institute for High Energy Physics, Protvino, Russia. Member of the Russian collaboration to the LHC Project.

around the beam elements are computed to estimate both possible radiation damage to the coil insulation and radiation levels along the cleaning section. The design of the shielding and induced radioactivity levels will be presented in a following report.

2 The momentum cleaning insertion in IR3

2.1 The layout of the cleaning section

The principles of optics used for a momentum cleaning insertion can be found in [2, 7, 8]. The primary collimation has to preserve the full nominal transverse beam size in the momentum range of the RF bucket. At the same time the momentum distribution of the halo must be restricted to the stable momentum range and to the momentum aperture of the ring. The dispersion at the primary collimator must be as large as possible to protect the arc. Moreover the effective relative retraction between the primary and the secondary collimators must be made independent of the momentum deviation, in order to ensure that the maximum amplitude of the secondary halo is equal for all momentum deviations δ_p.

The cleaning section consists mostly of conventional magnets to avoid quenches and high heat loads to cryogenics. Only two out of six quadrupoles are superconducting, namely Q6L upstream and Q6R far downstream of the collimators. Each of them consists of five MQTL modules (V6.2). A pair of warm bending magnets (D4L, D3L) increases the beam separation locally from 194 to 224 mm and another pair (D3R, D4R) restores the nominal separation. These dipoles consist each of three MBW modules. Each of the warm quadrupoles Q4L(R) and Q5L(R) consists of five MQWA modules and one MQWB module. Both types of modules have the same mechanical design. Horizontal MCH and vertical MCV correctors consist of one warm MCBW dipole.

The full list of the collimators and magnets at their longitudinal positions in the momentum cleaning section is given in Table 1.

The primary losses are shared between 1 primary and 6 secondary collimators for each ring. Both primary and secondary collimators have a similar mechanical design but their jaws are different. Jaws of primary collimators are made of aluminium and their length is 200 mm. Secondary collimators have 500 mm long jaws made of copper. In contrast to the betatron halo which spreads from the beam in all tranverse directions, momentum losses are concentrated in the horizontal plane. Therefore the primary collimator is horizontal. The individual positions of the collimators with respect to the axis of Beam 1 are given in Table 2.

2.2 The map of primary inelastic collisions

The K2 code [1, 9] is used to prepare a map of primary inelastic interactions in the collimator jaws. A proton with initial nonzero δ_p and no betatronic amplitude is circulated inside the primary aperture using one turn linear motion. Turn after turn, a small increment is added to the betatronic amplitude until a collimator is touched. Then scattering in the collimators and tracking with linear betatron motion between collimators are continued. In the collimators a Monte-Carlo method is used to simulate nuclear and electromagnetic elastic scattering. Multiple Coulomb scattering is treated as a continuous diffusion process, carefully iterating

Table 1: Sequence of elements of the cleaning insertion. The upstream longitudinal position of the elements (entrance) and their length correspond to the optics version V6.2.

Name	Entrance [m]	Length [m]	Element description, type of modules
Q6L.E	0.000	1.300	Cold quadrupole, MQTL
Q6L.D	1.595	1.300	Cold quadrupole, MQTL
Q6L.C	3.190	1.300	Cold quadrupole, MQTL
Q6L.B	4.786	1.300	Cold quadrupole, MQTL
Q6L.A	6.381	1.300	Cold quadrupole, MQTL
D4L.F	11.119	3.400	Warm separation dipole, MBW
D4L.E	15.193	3.400	Warm separation dipole, MBW
D4L.D	19.267	3.400	Warm separation dipole, MBW
TCP1	27.090	0.200	Primary collimator of Ring 1, TCP
D3L.C	37.612	3.400	Warm separation dipole, MBW
D3L.B	41.686	3.400	Warm separation dipole, MBW
D3L.A	45.760	3.400	Warm separation dipole, MBW
MCV.Q5L	50.999	1.700	Dipole corrector vertical of Ring 1, MCBW
Q5LA.E	53.420	3.108	Warm quadrupole, MQWA
TCS1	57.000	0.500	Secondary collimator of Ring 1, TCS
Q5LA.D	58.120	3.108	Warm quadrupole, MQWA
Q5LA.C	61.820	3.108	Warm quadrupole, MQWA
Q5LB.0	65.520	3.108	Warm quadrupole, MQWB
Q5LA.B	69.220	3.108	Warm quadrupole, MQWA
Q5LA.A	72.920	3.108	Warm quadrupole, MQWA
MCH.Q5L	76.749	1.700	Dipole corrector horizontal of Ring 2, MCBW
TCS6/2	139.130	0.500	Secondary collimator of Ring 2, TCS
TCS5/2	144.370	0.500	Secondary collimator of Ring 2, TCS
TCS4/2	150.190	0.500	Secondary collimator of Ring 2, TCS
MCH.Q4L	155.280	1.700	Dipole corrector horizontal of Ring 1, MCBW
Q4LA.E	157.701	3.108	Warm quadrupole, MQWA
TCS3/2	161.426	0.500	Secondary collimator of Ring 2, TCS
TCS2/2	162.426	0.500	Secondary collimator of Ring 2, TCS
Q4LA.D	163.401	3.108	Warm quadrupole, MQWA
Q4LA.C	167.101	3.108	Warm quadrupole, MQWA
Q4LB.0	170.801	3.108	Warm quadrupole, MQWB
Q4LA.B	174.501	3.108	Warm quadrupole, MQWA
Q4LA.A	178.201	3.108	Warm quadrupole, MQWA
MCV.Q4L	182.030	1.700	Dipole corrector vertical of Ring 2, MCBW
MCV.Q4R	225.500	1.700	Dipole corrector vertical of Ring 1, MCBW
Q4RA.A	227.971	3.108	Warm quadrupole, MQWA
Q4RA.B	231.671	3.108	Warm quadrupole, MQWA
Q4RB.0	235.371	3.108	Warm quadrupole, MQWB
Q4LA.C	239.071	3.108	Warm quadrupole, MQWA
Q4LA.D	242.771	3.108	Warm quadrupole, MQWA
TCS2	246.354	0.500	Secondary collimator of Ring 1, TCS
TCS3	247.354	0.500	Secondary collimator of Ring 1, TCS
Q4LA.E	248.471	3.108	Warm quadrupole, MQWA
MCH.Q4R	252.300	1.700	Dipole corrector horizontal of Ring 2, MCBW
TCS4	258.590	0.500	Secondary collimator of Ring 1, TCS
TCS5	264.410	0.500	Secondary collimator of Ring 1, TCS
TCS6	269.650	0.500	Secondary collimator of Ring 1, TCS
MCH.Q5R	330.831	1.700	Dipole corrector horizontal of Ring 1, MCBW

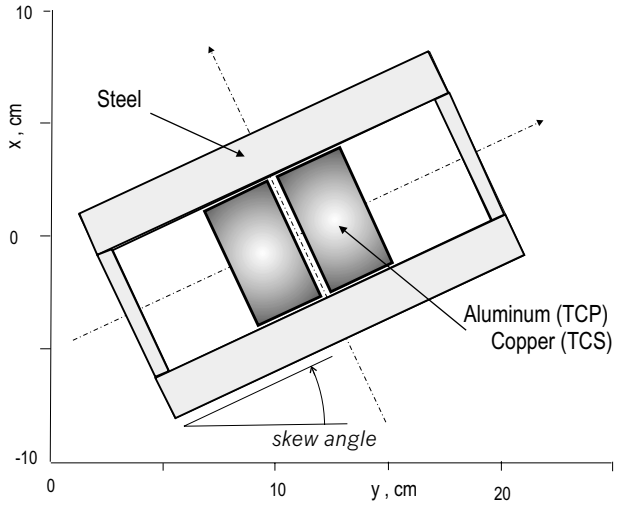

Figure 1: The cross-section of a collimator tank, as used in the simulation .

Table 1 - continued

Name	Entrance [m]	Length [m]	Element description, type of modules
Q5RA.A	333.252	3.108	Warm quadrupole, MQWA
Q5RA.B	336.952	3.108	Warm quadrupole, MQWA
Q5RB.0	340.652	3.108	Warm quadrupole, MQWB
Q5RA.C	344.352	3.108	Warm quadrupole, MQWA
Q5RA.D	348.052	3.108	Warm quadrupole, MQWA
TCS1/2	351.775	0.500	Secondary collimator of Ring 2, TCS
Q5RA.E	352.752	3.108	Warm quadrupole, MQWA
MCV.Q5R	356.581	1.700	Dipole corrector vertical of Ring 2, MCBW
D3R.A	360.120	3.400	Warm separation dipole, MBW
D3R.B	364.194	3.400	Warm separation dipole, MBW
D3R.C	368.268	3.400	Warm separation dipole, MBW
TCP1/2	381.990	0.200	Primary collimator of Ring 2, TCP
D4R.D	386.613	3.400	Warm separation dipole, MBW
D4R.E	390.687	3.400	Warm separation dipole, MBW
D4R.F	394.761	3.400	Warm separation dipole, MBW
Q6R.A	401.599	1.300	Cold quadrupole, MQTL
Q6R.B	403.194	1.300	Cold quadrupole, MQTL
Q6R.C	404.790	1.300	Cold quadrupole, MQTL
Q6R.D	406.385	1.300	Cold quadrupole, MQTL
Q6R.E	407.980	1.300	Cold quadrupole, MQTL

Table 2: Transverse collimator positions for the optics V6.2 in Ring 1. The radius is the shortest distance between the beam axis and the jaw. The convention for the skew angle is shown in Figure 1. The skew angles are chosen for best capture of the secondary protons and depend on the two phase advances between the primary and the secondary collimator [2].

Collimator	Injection		Collision	
	skew angle [rad]	radius [cm]	skew angle [rad]	radius [cm]
TCP1	0.00000	0.5862	0.00000	0.14860
TCS1	0.00000	0.4177	0.00000	0.10590
TCS2	0.07920	0.3320	0.07920	0.08418
TCS3	-0.07826	0.3315	-0.07826	0.08407
TCS4	-0.15520	0.3955	-0.15520	0.10020
TCS5	0.16960	0.4328	0.16960	0.10970
TCS6	-0.15640	0.4630	-0.15640	0.11760

Table 3: The relative rates of inelastic interactions in the collimator jaws. The sum over the collimators is equal to 1.

	TCP1	TCS1	TCS2	TCS3	TCS4	TCS5	TCS6
Injection	0.431	0.211	0.183	0.104	0.034	0.030	0.007
Collisions	0.760	0.059	0.078	0.054	0.022	0.022	0.005

the motion near the edge of the jaw to avoid non-physical trajectories. Tracking is stopped as soon as an inelastic interaction occurs in one of the collimators and the coordinates of the proton at the interaction point are stored. The full map of inelastic interactions is obtained by tracking thirty thousand protons.

The calculated relative rates of inelastic interactions in the collimator jaws are presented in Table 3.

3 Cascade simulations

Hadron and electromagnetic cascade development is simulated using the Monte-Carlo code MARS [10]. The extended standard geometry language of the MARS code [11] is used to present the momentum cleaning section as a sequence of elements corresponding to the IR3 layout in version V6.2.

The geometry starts at the entrance of quadrupole Q6L and ends at the end of the quadrupole Q6R. One longitudinal half of the geometry is shown schematically in Figure 2. The z-axis of the right Cartesian coordinate system (x, y, z) coincides with the longitudinal axes of all the twin aperture magnets and lies in the plane of the beams exactly between them, while the x and y axes look up and inside the ring correspondingly.

Every collimator tank is presented as a pair of jaws in a vacuum box as shown in Figure 1. Both primary and secondary collimators have the same transverse cross-section but they are different in length and the material of the jaws.

The transverse cross-sections of dipoles and quadrupoles are shown in Figures 3,4,5 and 6. Except for minor changes in their dimensions, the cross-sections of the body of MBW and MCBW dipoles are identical to the one used in [4] for cascade simulations in IR7. However there is a significant difference with [4] at the coil ends. In [4] the front and rear protruding ends of the coils were assumed to be bent away from the beam plane. In the current design of the MBW [12] the coils are flat even at their returning ends ('racetrack coils'), where they therefore pass close above the beam pipes. The coils of the MCBW are also flat over all their length. As we will show below, higher doses must therefore be expected in the protruding parts of the dipole coils which are not protected by the magnet yoke.

The beam pipes in the short drift spaces between magnet modules are similar to those installed inside the magnets. In the long drift spaces, we used beam pipes made of copper tubes with 100 mm inner diameter and 105 mm outer diameter. Vacuum pumps, flanges and bellows are not taken into account in the present set of simulations.

Dipole fields and quadrupole gradients in the apertures of D3, D4, Q4, Q5 and Q6, the magnetic lengths of the modules and the drift spaces between the modules are taken in a full accordance with the optics version V6.2.

An individual cascade starts from the inelastic nuclear interaction of a proton inside one of the collimator jaws. The 4D-space coordinates and the momentum of primary protons at their interaction point are taken from the map file. One map contains a limited number of the interaction points ($\sim$30000) therefore it was used many times per one simulation run in order to get reasonably small statistical errors of the energy deposition density calculation in the magnet coils.

The fluence of secondary hadrons with an energy above 10 MeV is scored at a 410 m long

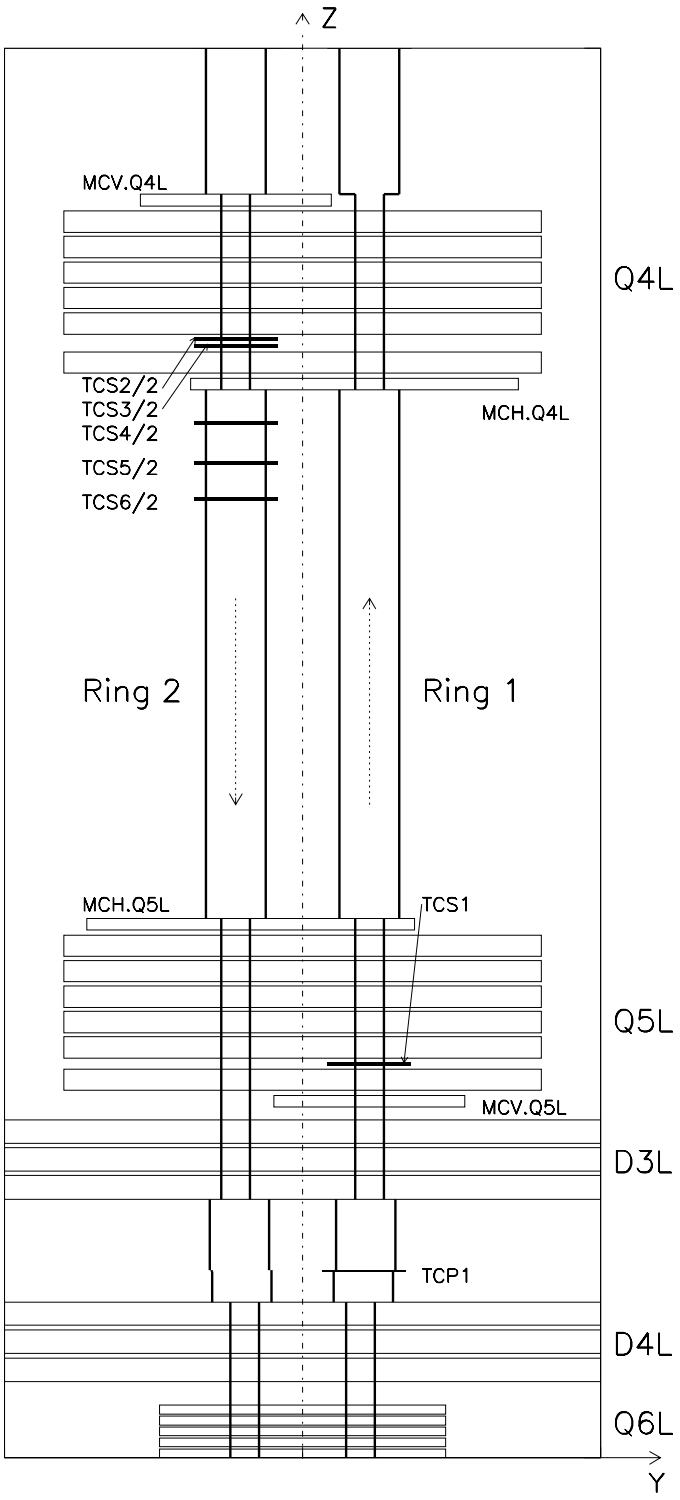

Figure 2: Layout of one half of the cleaning section, as presented in the MARS code.

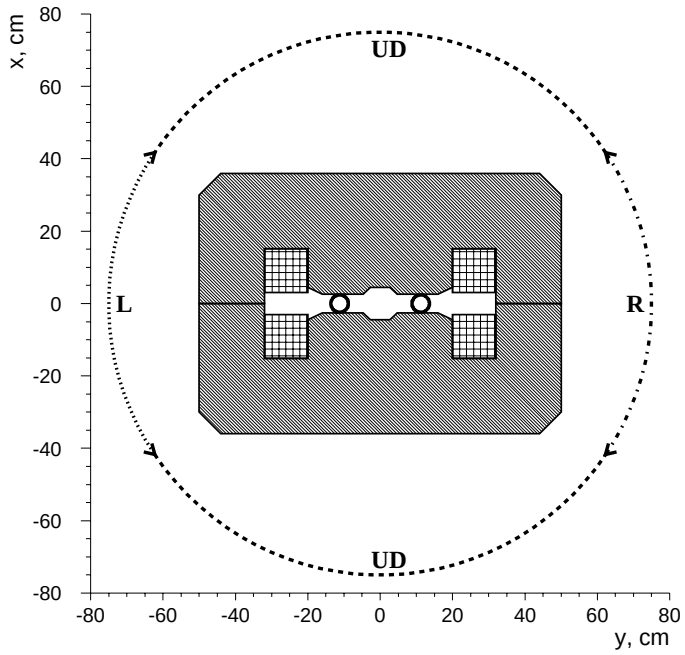

Figure 3: Cross-section of the warm dipole MBW with the scoring shell around it.

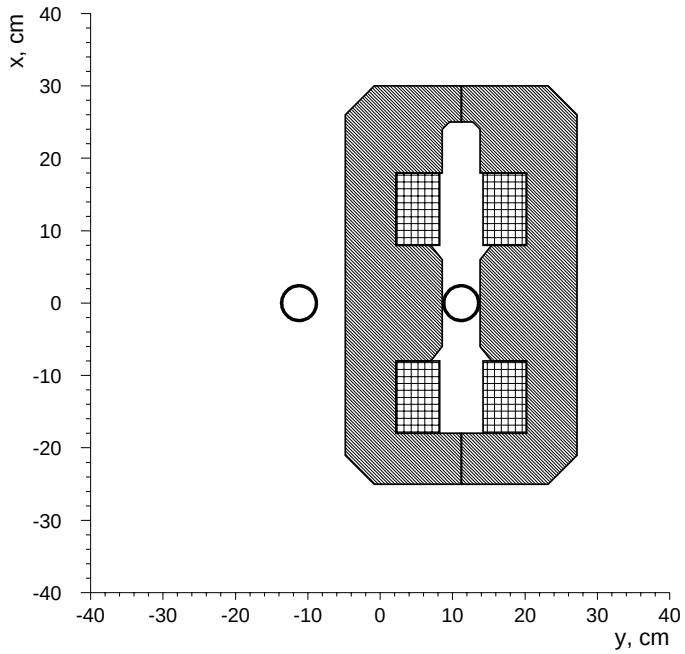

Figure 4: Cross-section of the warm dipole corrector MCBW in the vertical position.

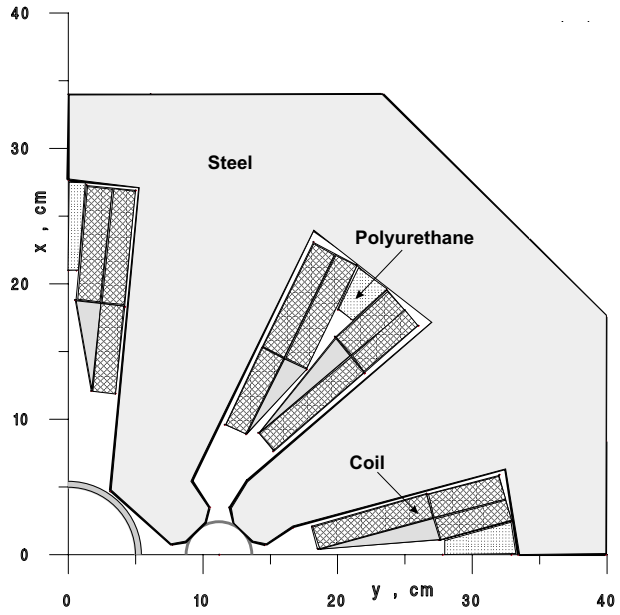

Figure 5: One quarter of the cross-section of the warm quadrupole MQWA(B).

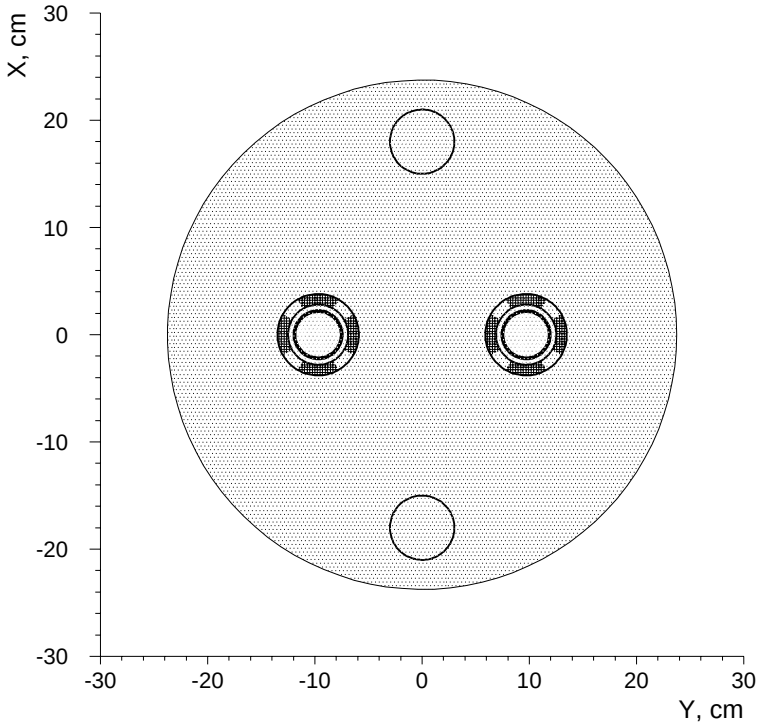

Figure 6: Cross-section of the cold quadrupole MQTL.

Table 4: Energy deposited in the jaws and in the tank proper and total power dissipated in each tanks. See Fig.1 for a cross-section of a collimator tank. The energy deposition corresponds to one proton lost in the collimators of one ring. The total power corresponds to a peak loss rate of $3 \cdot 10^9$ protons/s at collision energy.

Collimator	*injection* **Energy [GeV/proton]**		*collisions* **Energy [GeV/proton]**		**Total power [W]**
	jaws	tank	jaws	tank	*collisions*
TCP1	0.75	0.94	5.95	6.63	3.2
TCS1	37.2	39.9	1230.	1260.	606.
TCS2	26.1	28.6	318.	329.	158.
TCS3	24.2	27.5	317.	333.	160.
TCS4	7.14	7.94	136.	143.	68.6
TCS5	5.55	6.3	100.	107.	51.2
TCS6	2.06	2.5	45.7	49.4	23.7
All	103.	114.	2150.	2230.	1070.

cylindrical shell of 75 cm radius. The shell is subdivided both azimuthally (see Figure 3) and longitudinally with 1 metre segmentation. The radius and subdivisions of the scoring shell are the same as in [4].

4 Results

4.1 Energy deposition in the collimators

The calculated energy deposition per proton and the steady power deposition in the collimators is presented in Table 4. There is a high energy deposition in the secondary collimator TCS1 which absorbs both primary protons and secondary hadrons and photons produced in the primary collimator TCP. It is 40 times higher than in TCP at injection and 200 times higher at top energy. Energy deposition in TCS2 and TCS3 is also high. Radiation heating of the primary collimators at ramping was estimated in [13] as not negligible. Therefore a separate study is necessary to evaluate the thermal and mechanical robustness of the secondary collimators and the need of a cooling system.

4.2 Doses to the magnet coils

The annual doses are estimated from the calculated energy deposition densities in the magnet coils assuming the losses of 10^{16} 7 TeV protons in the momentum collimators of each Ring. The maximum doses to the magnet coils are given in the column "no shielding" of Table 5.

As it should be expected doses to the protruding front parts of MBW and MCBW coils adjacent to the beam pipe are the highest. They are equal to 18.5 MGy/year for the separation dipole D3 and 9.6 MGy/year for the vertical dipole corrector MCV upstream of the quadrupole Q5. These numbers are dangerously close to the maximum allowed dose of 50 MGy [12]. In a previous study [5] for the betatron cleaning section in IR7 the maximum

Table 5: Maximum annual absorbed dose in kGy to the coils of magnets of the momentum cleaning section. Doses correspond to 10^{16} 7 TeV protons lost in the momentum collimators of each Ring.

Magnet	**no shielding**	**with shielding**
Q6L.E	15	15
Q6L.D	25	25
Q6L.C	25	25
Q6L.B	40	40
Q6L.A	455	455
D4L.F	10	10
D4L.E	10	10
D4L.D	24	24
D3L.C	**18500**	**2100**
D3L.B	**2300**	**2100**
D3L.A	2200	2200
MCV.Q5L	**9600**	**4100**
Q5LA.E	330	330
Q5LA.D	1000	1000
Q5LA.C	180	180
Q5LB.0	100	100
Q5LA.B	60	60
Q5LA.A	60	60
MCH.Q5L	350	350
MCH.Q4L	**2900**	**900**
Q4LA.E	500	500
Q4LA.D	20	20
Q4LA.C	15	15
Q4LB.0	13	13
Q4LA.B	11	11
Q4LA.A	27	27
MCV.Q4L	**1000**	**700**

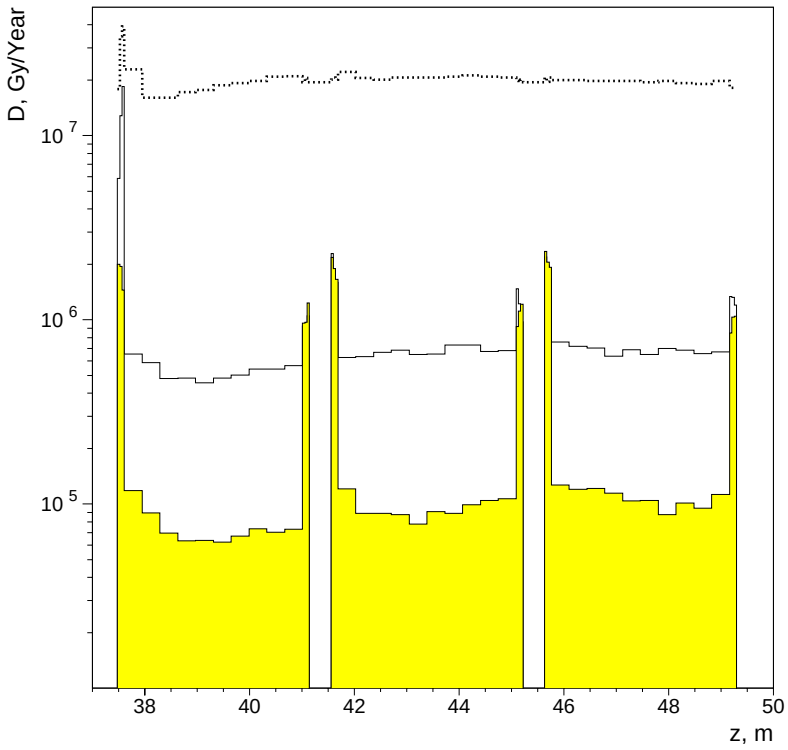

Figure 7: Annual doses along dipole D3 located near the primary collimators. Dotted clear histogram - dose in the beam pipe, solid clear histogram - maximum dose in the coils, grey histogram - maximum dose in the coils in the case of shielding screen upstream of D3 and shielding inserts inside D3.

doses of 4 MGy/year were reported for D3 and for the warm quadrupole downstream of D3. As we noted in Section 3, the protruding ends of the MBW coils were assumed in [5] to be bent up and down away from the beam plane so that they were not irradiated more than the rest of the coils.

Maximum values of doses in the coil transverse cross-section along all three modules of the dipole D3 are shown in Figure 7. In the coils inside the magnet yoke, the dose does not exceed 1 MGy/year while it is at least twice higher in the front and rear parts of the coils.

Shielding screens surrounding the beam pipe upstream of D3, MCV.Q5 and MCH.Q4 will reduce the doses to their front coils. Those adjacent to the beam pipes must not have larger cross-section than the pipe inside these magnets. We introduce screens made of iron and having the outer dimensions of the magnet. The length of the screen upstream of D3 is taken as 1 metre. The screens upstream of MCV.Q5 and MCH.Q4 are taken half as long. A clearance of 50 cm long is left between the screens and the downstream magnets for the vacuum equipment. In addition, the gaps of the D3 modules are filled with copper insertions as shown in Figure 8.

The results of the maximum annual dose calculations with the above screens and insertions are given in the column "with shielding" of the Table 5. In this case the highest dose among IR3 magnets is 4.1 MGy/year which occurs in the coils of the vertical correctors

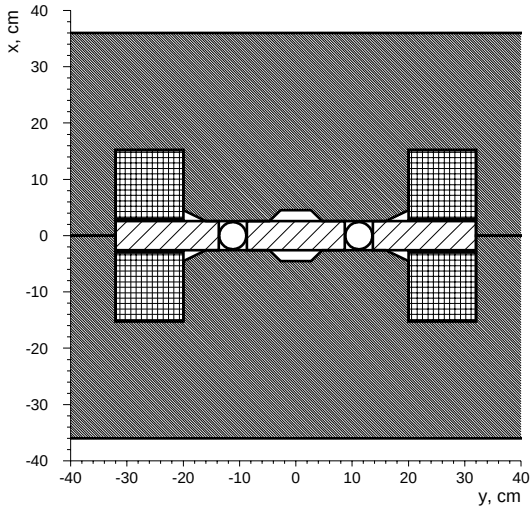

Figure 8: Cross-section of the warm dipole MBW with the shielding inserts.

MCV.Q5. This value ensures a lifetime of the coils of about 13 years. A further reduction of the annual dose to them would require to change the design of the MCBW modules.

A significant reduction of the maximum dose can be noted for D3 coils (see the solid shaded histogram in Figure 7). However neither the shielding screen upstream nor the shielding insertions inside reduce doses to the end parts of the coils (except for the front coils of the first module). This is explained by the fact that these parts of the coils are irradiated mostly by electromagnetic components of the cascades initiated by energetic secondaries from the TCP in the material of the beam pipe along the magnets. The intensity of these cascades is practically the same all along D3 without any peaks between the modules as can be seen from the dotted histogram showing the dose in the beam pipe in Figure 7. Therefore the reason for the higher doses in the end parts of the coils is that they are too close to the beam pipes. We conclude that for the present design of the MBW coils doses at their protruding ends cannot be reduced with use of shielding insertions inside these dipoles or extension of the distance between modules. But with an annual dose of 2 MGy/year, the lifetime is 25 years, which is an adequate value.

4.3 Power deposition to the superconducting quadrupoles Q6

Both power deposition density in the coils and heat load to the cryogenics are of interest for the superconducting quadrupoles Q6. Assuming a peak cleaning rate of $\dot{n} = 3 \cdot 10^9$ protons per second, we obtain a maximum density of power deposition of $w = 1.0$ mW/cm^3 in the coils of Q6 (the corresponding maximum annual dose is 0.46 MGy). This value of 1.0 mW/cm^3 is below the quench limit of 5 mW cm^{-3} from [14] but not too far from it.

Total energy deposited in Q6 is equal to 3 GeV per one 7 TeV proton absorbed by the cleaning system. Taking $1 \cdot 10^9$ protons per second as an average cleaning rate we come to the average power load of 0.48 W to the cryostat of Q6.

In a transient regime of losses ($\Delta t > 10$ ms), the nominal heat reserve of the cables is

Table 6: Longitudinally averaged parameters of hadron leakage in IR3 and IR7 : fluences $< F_L >$, $< F_R >$, $< F_{UD} >$ and $< F >$ in the left, right, upper/bottom segments of the scoring shell and in the entire shell, correspondingly; leakage energy E_s and average energy of hadron spectrum $< E >$.

Mode	Insertion	$< F_L >$ cm^{-2}	$< F_{UD} >$ cm^{-2}	$< F_R >$ cm^{-2}	$< F >$ cm^{-2}	E_s GeV	$< E >$ MeV
Collisions	IR3	$1.63 \cdot 10^{-4}$	$1.88 \cdot 10^{-4}$	$2.74 \cdot 10^{-4}$	$2.00 \cdot 10^{-4}$	500	230
	IR7	$1.73 \cdot 10^{-4}$	$2.11 \cdot 10^{-4}$	$2.89 \cdot 10^{-4}$	$2.20 \cdot 10^{-4}$	802	380
Injection	IR3	$2.04 \cdot 10^{-5}$	$2.62 \cdot 10^{-5}$	$3.61 \cdot 10^{-5}$	$2.70 \cdot 10^{-5}$	64	250
	IR7	$2.15 \cdot 10^{-5}$	$2.77 \cdot 10^{-5}$	$3.41 \cdot 10^{-5}$	$2.77 \cdot 10^{-5}$	93	350

$\Delta Q = 3 \times 10^{-2}$ J/cm^3 at high field [14]. With $\dot{n} = 3 \cdot 10^9$ p/s $\equiv$ w $= 10^{-3}$ W, it follows that the allowed integrated transient loss is $\Delta n = \dot{n} \Delta Q / w = 9 \times 10^{11}$ p, or $3^\circ/_{\circ\circ}$ of a nominal coast. A similar calculation remains to be done at injection energy.

4.4 Hadron leakage

The longitudinal distributions of hadron fluence in the scoring shell are shown in Figure 9. They have practically the same shape at injection and at top energy with maxima corresponding to the collimator locations. The most prominent narrow peaks correspond to the secondary colimators TCS1 and TCS2+TCS3 located between the modules of the warm quadrupoles Q5 and Q4.

Parameters of average lateral leakage are given in Table 6 in comparison with the corresponding data from [4] for the betatron cleaning section in IR7. The average fluences are practically the same as in IR7 and the leakage energies are noticeably lower. This is explained by the location of TCS1-TCS3 between the quadrupole modules while in [4] all the collimators were located in the long drift spaces. For the same reason the efficiency of shielding in IR3 can be lower than the results for the shielding efficiency in IR7 from [4].

The integral spectra of hadrons and photons downstream Q6R at top energy are shown in Figure 10. An analysis of the integral leakage spectra downstream Q6R allows to determine both efficiency of the momentum cleaning system and possible radiation impact on the superconducting quadrupole Q7R. As can be seen from Figure 10 the proton spectrum is almost constant in the energy range from 1 GeV up to 1000 GeV, and is the main contribution to the integral spectrum above 1000 GeV. The integrated efficiency of the momentum cleaning system, defined here as the flux of energy leaving the insertion divided by the one intercepted by the collimators, is equal to 10^{-3} and $5 \cdot 10^{-4}$ for hadrons with energy larger than 1000 GeV and 6000 GeV, respectively.

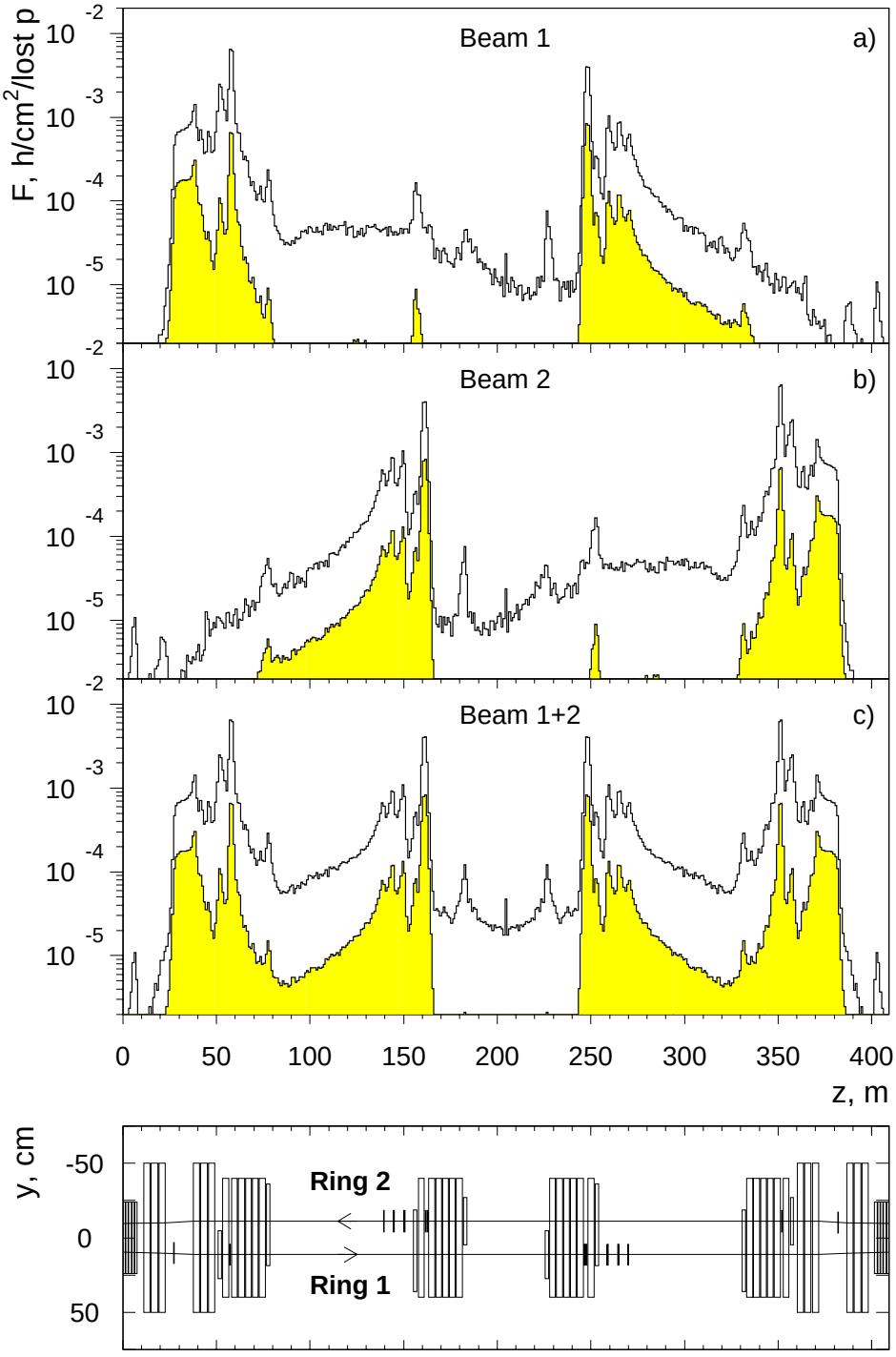

Figure 9: Fluence of hadrons in the scoring shell around the momentum cleaning section in IR3: (a) – per proton of Beam 1 lost in the momentum collimators of Ring 1, (b) – per proton of Beam 2 lost in the momentum collimators of Ring 2, (c) – the sum of (a) and (b). The case of cleaning at top energy is shown by the clear histogram, the grey histogram is for cleaning at injection.

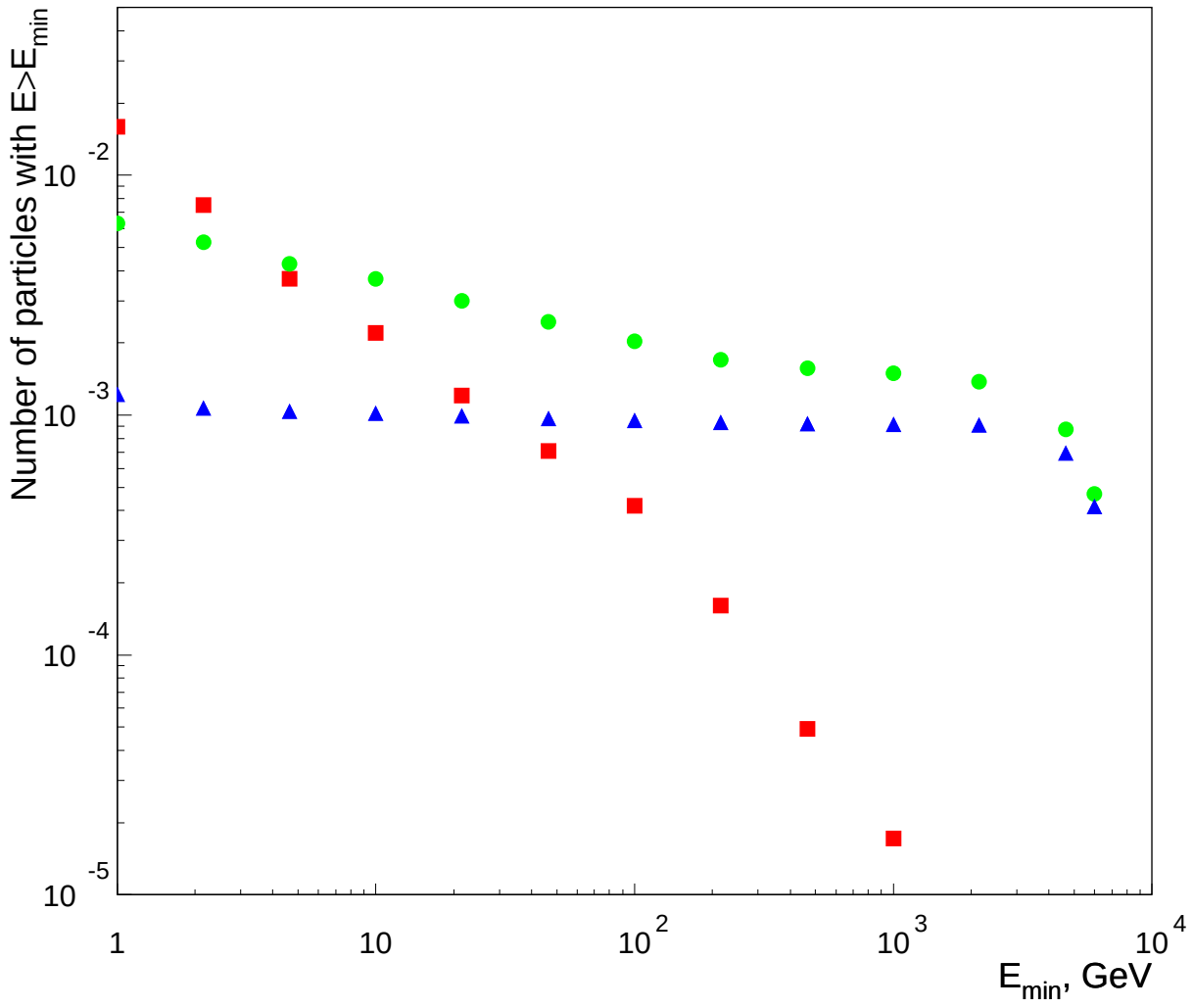

Figure 10: The Integral spectra of hadrons and photons downstream Q6R at top energy: square– photons, circle – all hadrons, triangular – protons. The number of particles is normalised to one inelastically lost proton in the insertion.

5 Conclusions

We can summarise our main results as follows.

- A thermal study is necessary to examine the robustness of the secondary collimator.
- Without shielding, doses to coils of the both D3L dipole and MCV.Q5L vertical corrector dipole are dangerously close to the maximum allowed dose of 50 MGy.
- Shielding screens in front of D3L, MCV.Q5L and MCH.Q4L modules allow to reduce doses to the coils down to 2.2 MGy/yr, 4.1 MGy/yr and 0.9 MGy/yr respectively. The same screens shall of course be installed symmetrically on the right side of IP3 to protect the magnets against losses associated to beam 2.
- Apart from the cases discussed above, and with the present design of the MBW coils, doses at their front and rear ends cannot be reduced by using shielding screens and inserts. But, on the other hand, the worst annual dose simulated is 2.2 MGy/yr (MBW), while it never exceeds 1 MGy/yr in MQW's.
- A further reduction of dose level in coils of the MCV.Q5L vertical corrector dipole would require a design change of the MCBW.
- The maximum power deposition density in the coils of Q6 is 1.0 mW cm^{-3}.
- The optimal shielding remains to be studied.
- The integrated efficiency of the momentum cleaning system at top energy and for the high energy component of the tertiary flux is $5 \cdot 10^{-4}$.

References

[1] N. Catalan Lasheras et al., *Proton Collimation in TeV Colliders*, CERN LHC Project Report 156, 1997.

[2] J.B. Jeanneret, *Optics of a two-stage collimation system*, Phys. Rev. ST-AB, **1**,081001, 1998, and CERN LHC Project Report 243, 1997.

[3] G.R. Stevenson, A. Fasso and J.M. Zazula, *Estimation of parameters of radiological interest for the scraper system of the LHC*, CERN Internal Report CERN/TIS-RP/IR/92-25, 1992.

[4] I. Azhgirey, I. Baishev, N. Catalan Lasheras and J.B. Jeanneret, *Cascade simulations for the betatron cleaning insertion*, CERN LHC Project Note 121, 1997; CERN LHC Project Report 184, 1998.

[5] I. Azhgirey, I. Baishev and J.B. Jeanneret, *Energy deposition calculations for the betatron cleaning insertion of LHC*,CERN LHC Project Note 171, 1998.

[6] I.L. Azhgirey et al., *Radiation studies of the LHC betatron scraping region at point 7*, CERN Internal Report CERN/TIS-RP/IR/99-01, 1999.

[7] J.B. Jeanneret, *A specification for the momentum cleaning*, LHC Project Note 115, 1997.

[8] D.I. Kaltchev, M.K. Craddock, R.V. Servranckx and T. Risselada, *Momentum Cleaning in the CERN LHC*, CERN LHC Project Report 194, 1998.

[9] T. Trenkler and J.B. Jeanneret, *K2: A software package evaluating collimation systems in circular colliders (Manual)*, CERN Internal Report SL/AP Note 94-105, 1994.

[10] I.L. Azhgirey, I.A. Kurochkin and V.V. Talanov, *MARS program complex development for radiation aspects of electro-nuclear devices design*, in: *Materials of XV Workshop on Charged Particle Accelerators*, Vol. 2, p. 270, Protvino, 1996 (in Russian).

[11] V.V. Talanov, *Universal Geometrical module for MARS Program*, Preprint IHEP 92-99, Protvino, 1992 (in Russian).

[12] *Technical specification for the MBW separation dipole for the LHC beam cleaning insertions*, LHC Project document LHC-MBW-CA-002, Rev.1/20-12-2000.

[13] I. Baishev, A. Barsukov and J.B. Jeanneret, *Radiation heating of primary collimators at ramping*, CERN LHC Project Report 309, 1999.

[14] J.B. Jeanneret et al., *Quench levels and transient beam losses in LHC magnets* CERN LHC Project Report 44, 1996.

[15] M. Höfert, K. Potter and G.R. Stevenson, *Summary of Design Values, Dose Limits, Interaction Rates etc. for use in estimating Radiological Quantities associated with LHC Operation*, CERN Internal Report CERN/TIS-RP/IR/95-19.1, 1995.